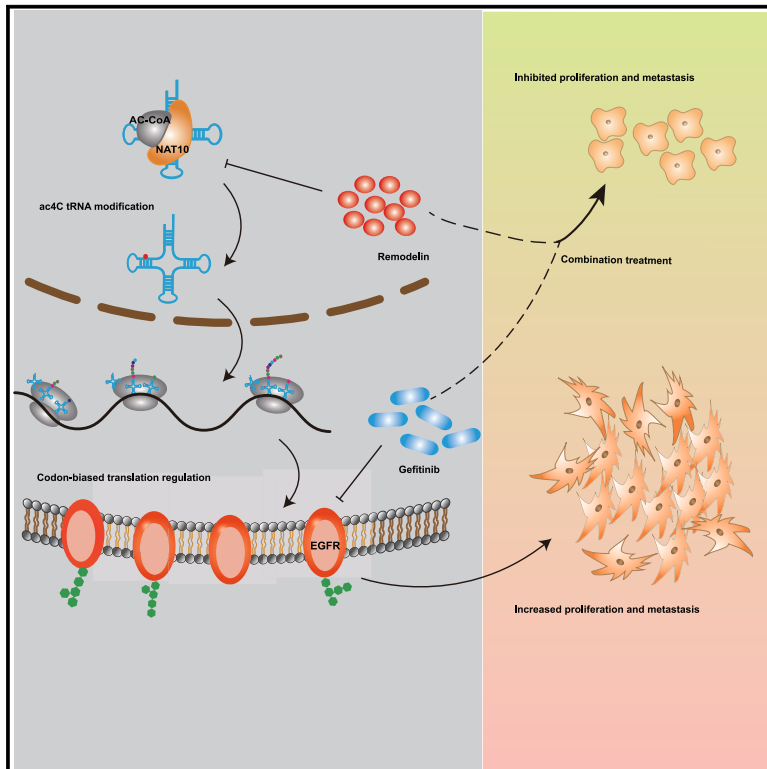# Cell Reports

NAT10-mediated ac4C tRNA modification promotes EGFR mRNA translation and gefitinib resistance in cancer

Graphical abstract

Authors

Wei Wei, Shuishen Zhang, Hui Han, ..., Lianlian Liu, Junho Choe, Shuibin Lin

Correspondence

linshb6@mail.sysu.edu.cn

In brief

Wei et al. found that NAT10-mediated ac4C tRNA modification promotes the development of esophageal cancer by enhancing the translation efficiency of EGFR. The combination of gefitinib and remodelin, a small-molecule inhibitor of NAT10, showed great potential for the treatment of esophageal cancer.

Highlights

- NAT10 enhances tRNA stability through ac4C modification

- NAT10 promotes esophageal cancer development by enhancing the translation efficiency of EGFR

- Inhibition of NAT10 enhances the effectiveness of gefitinib treatment in esophageal cancer

CellPress

Article

NAT10-mediated ac4C tRNA modification promotes EGFR mRNA translation and gefitinib resistance in cancer

Wei Wei,[1,11] Shuishen Zhang,[2,11] Hui Han,[1,11] Xiaochen Wang,[1,11] Siyi Zheng,[1] Zhaoyu Wang,[1] Chunlong Yang,[3] Lu Wang,[4] Jieyi Ma,[1] Siyao Guo,[1] Juan Wang,[5] Lianlian Liu,[6] Junho Choe,[7,8,9,10] and Shuibin Lin[1,12,*]

[1]Department of Otolaryngology, Center for Translational Medicine, Precision Medicine Institute, The First Affiliated Hospital of Sun Yat-sen University, Guangzhou 510080, China
[2]Department of Thoracic Surgery, The First Affiliated Hospital, Sun Yat-sen University, Guangzhou 510080, China
[3]Clinical Research Center, Affiliated Hospital of Guangdong Medical University, Zhanjiang 524001, China
[4]Department of Medical Laboratory, School of Laboratory Medicine and Biotechnology, Southern Medical University, Guangzhou 510515, China
[5]Division of Pulmonary and Critical Care Medicine, The First Affiliated Hospital of Sun Yat-sen University, Guangzhou 510080, China
[6]Department of Oral and Maxillofacial Surgery, The First Affiliated Hospital of Sun Yat-sen University, Guangzhou 510080, China
[7]Department of Life Science, College of Natural Sciences, Hanyang University, Seoul 04763, Republic of Korea
[8]Research Institute for Natural Sciences, Hanyang University, Seoul 04763, Republic of Korea
[9]Hanyang Institute of Bioscience and Biotechnology, Hanyang University, Seoul 04763, Republic of Korea
[10]Research Institute for Convergence of Basic Sciences, Hanyang University, Seoul 04763, Republic of Korea
[11]These authors contributed equally
[12]Lead contact
*Correspondence: linshb6@mail.sysu.edu.cn
https://doi.org/10.1016/j.celrep.2023.112810

SUMMARY

Aberrant RNA modifications are frequently associated with cancers, while the underlying mechanisms and clinical significance remain poorly understood. Here, we find that the ac4C RNA acetyltransferase NAT10 is significantly upregulated in esophageal cancers (ESCAs) and associated with poor ESCA prognosis. In addition, using ESCA cell lines and mouse models, we confirm the critical functions of NAT10 in promoting ESCA tumorigenesis and progression *in vitro* and *in vivo*. Mechanistically, NAT10 depletion reduces the abundance of ac4C-modified tRNAs and decreases the translation efficiencies of mRNAs enriched for ac4C-modified tRNA-decoded codons. We further identify EGFR as a key downstream target that facilitates NAT10's oncogenic functions. In terms of clinical significance, we demonstrate that NAT10 depletion and gefitinib treatment synergistically inhibit ESCA progression *in vitro* and *in vivo*. Our data indicate the mechanisms underlying ESCA progression at the layer of mRNA translation control and provide molecular insights for the development of effective cancer therapeutic strategies.

INTRODUCTION

Esophageal cancer (ESCA) is an invasive and malignant tumor that causes more than 400,000 deaths worldwide each year.[1] Because ESCAs are often diagnosed at advanced stages and current treatment options for advanced ESCA are limited, the overall prognosis of ESCA is poor, and the mortality rate remains high.[2–4] Recent clinical trials revealed that the EGFR inhibitor gefitinib showed an overall survival benefit in a subgroup of patients with advanced ESCA[5–8]; however, the overall response rate is limited. Therefore, it is urgent to investigate the molecular mechanisms underlying ESCA progression and drug resistance for the development of effective ESCA therapeutic strategies.

The pathogenic mechanisms underlying ESCA progression and drug resistance are complicated. Genetic amplifications or mutations of important oncogenes or tumor suppressors can lead to aberrant expression or functions of oncogenic factors in ESCA.[9] In addition, epigenetic modifications on DNA or histone proteins result in mis-regulations of oncogenic factors at gene transcription steps.[10,11] Recent emerging studies uncovered that RNA modifications play important functions in the regulation of gene expression and ESCA progression.[12–14] There are more than 100 types of RNA modifications,[15] and mis-regulated RNA modification enzymes are frequently found in cancers,[16–18] while the roles of RNA modifications in ESCA progression remain poorly understood.

The ac4C modification is a conserved chemically modified nucleoside present on different types of RNAs.[19,20] NAT10 is the only enzyme known to catalyze ac4C RNA modification, which regulates gene expression by modulating RNA stability
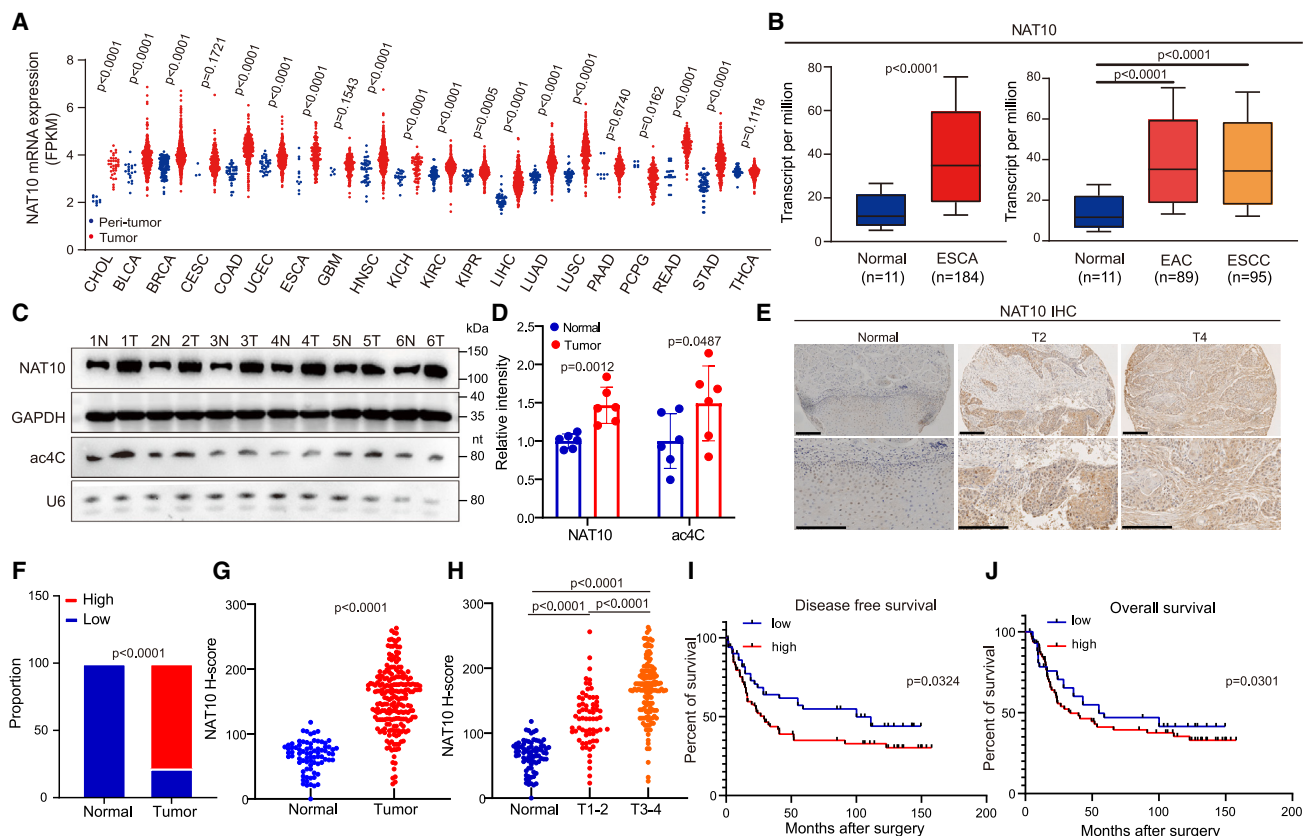
Figure 1. NAT10 is upregulated in ESCA and associated with poor ESCA prognosis

(A) NAT10 mRNA expression between tumor and peritumor tissues in 20 cancer types from TCGA datasets.

(B) Comparison of mRNA levels of NAT10 in ESCA with healthy tissues in TCGA-ESCA dataset (n = 11 in healthy, n = 184 in ESCA, n = 89 in EAC, n = 95 in ESCC).

(C and D) Blotting and quantitative analysis of NAT10 and tRNA ac4C levels in ESCA tumors and healthy tissues (N, normal; T, tumor; n = 6).

(E) Representative images of NAT10 IHC staining in ESCA and healthy tissues. Scale bar, 200 μm.

(F) Percentage of high NAT10 expression sample and low NAT10 expression sample in healthy or ESCA tissues.

(G and H) Quantification of NAT10 H-score for overall or different grades in ESCA and healthy tissues.

(I and J) Kaplan-Meier analysis for the disease-free survival and overall survival of patients with ESCA based on NAT10 H-scores.

For histograms, each point represents an independent experiment, and the data are shown as the mean ± SD with p values labeled on individual panels. p values were calculated by two-tailed unpaired Student's t test (A, D, G, and H) and log rank test (I and J).

and translation efficiency.[21,22] Recent studies have shown that aberrant regulations of NAT10 and ac4C RNA modification are associated with disease progression including in cancers.[23–29] However, little is known about the roles of NAT10 and ac4C RNA modification in ESCA.

This study demonstrated that NAT10 is significantly up-regulated in ESCA and correlates with poor prognosis of patients with ESCA. The elevated NAT10 expression promotes ESCA progression *in vitro* and *in vivo*. Mechanistically, NAT10 depletion decreases ac4C modification and expression of tRNAs, leading to impaired translation of mRNAs (including *EGFR*) enriched with ac4C tRNA-decoded codons. In addition, we further uncovered that the combination of NAT10 inhibition and EGFR inhibitor gefitinib treatment synergistically blocks ESCA progression *in vitro* and *in vivo*. Our data provided a molecular basis for the development of therapeutic strategies for ESCA treatment.

RESULTS

NAT10 is upregulated in cancers and associated with poor esophageal carcinoma prognosis

To investigate whether NAT10 and ac4C RNA modification play significant roles in cancer progression, we first analyzed the mRNA levels of NAT10 in different cancer types using The Cancer Genome Atlas (TCGA) datasets. We found that NAT10 is significantly more up-regulated in diverse tumor tissues than in control tissues (Figure 1A). Further analysis revealed that mRNA levels of NAT10 are significantly elevated in both subtypes of ESCAs (Figure 1B). We further verified the association between NAT10 and the development of ESCA using clinical samples. The results showed that the levels of NAT10 and ac4C modification on tRNAs are significantly higher in tumor tissues compared with control tissues (Figures 1C and 1D). In addition, immunohistochemistry staining using esophageal
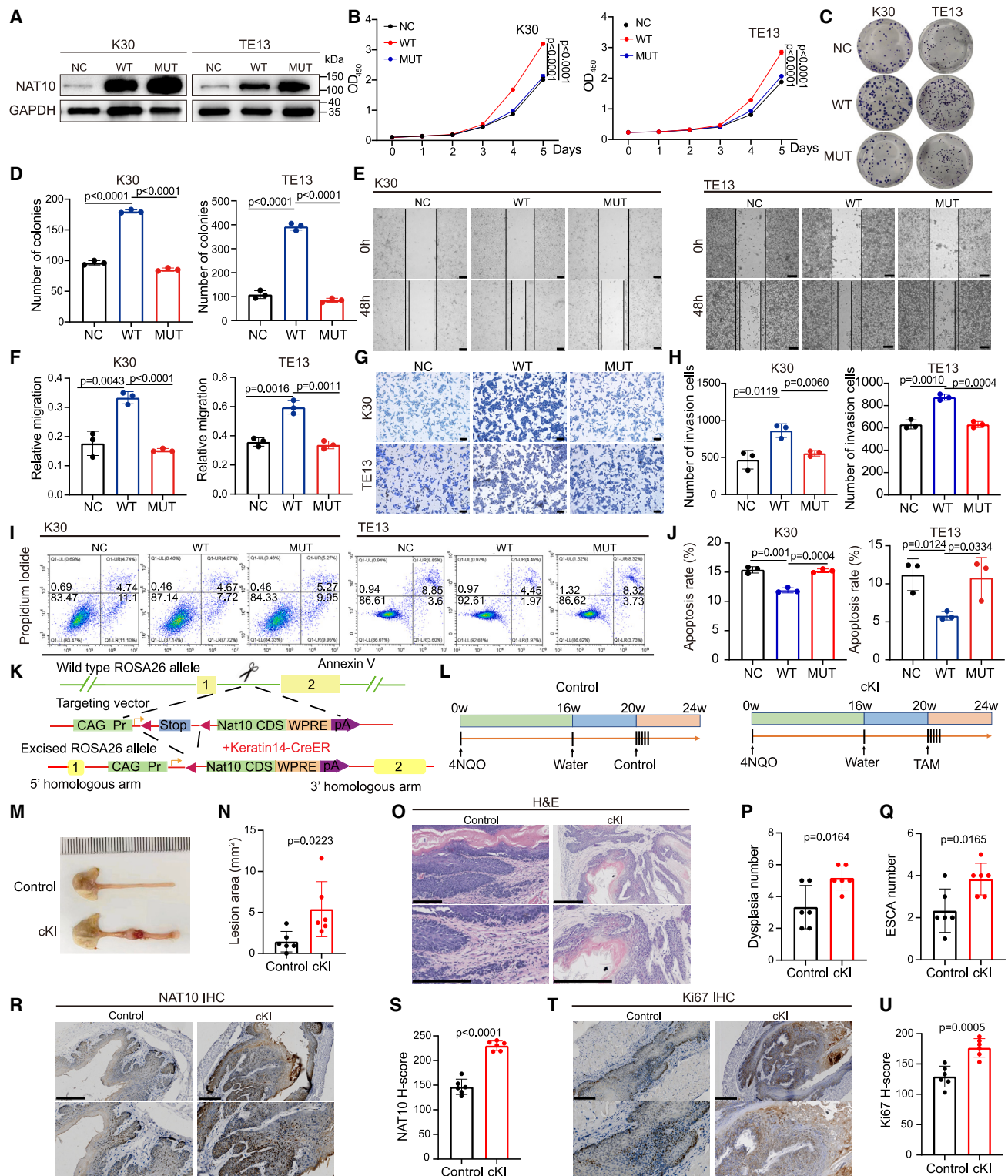
Figure 2. NAT10 promotes ESCA progression *in vitro* and in cKI mice

(A) The levels of NAT10 in TE13 and K30 cells after overexpression of WT NAT10 (WT) and the catalytic dead mutant of NAT10 (MUT).

(B) CCK8 assay of cell proliferation in NC, WT, and MUT ESCA cells. (n = 3).

(C and D) Representative images (C) and quantitative analysis (D) of colony formation in NC, WT, and MUT ESCA cells.

(E and F) Representative images (E) and quantitative analysis (F) of wound healing in NC, WT, and MUT ESCA cells. Scale bar, 200 μm.

(legend continued on next page)

carcinoma tissue arrays revealed that NAT10 is significantly up-regulated in tumor tissues and that high NAT10 expression is positively correlated with advanced tumor grades (Figures 1E–1H). In addition, we analyzed the prognosis of patients with ESCA and found that high expression of NAT10 is also significantly associated with poor patient prognosis (Figures 1I and 1J). Overall, our data suggested that NAT10 could have crucial oncogenic functions in the regulation of esophageal carcinoma.

NAT10 promotes ESCA progression *in vitro* and in conditional knockin mice

To explore the role of NAT10 in ESCA progression, we first performed gain-of-function assays using two NAT10 low-expressing ESCA cells, KYSE-30 and TE13 (Figure 2A). Our results showed that overexpression of wild-type (WT) NAT10 increased tRNA ac4C modification and significantly promoted the proliferation and colony-formation capacities of KYSE-30 and TE13 cells, while the catalytic dead mutant of NAT10 (Gly 641 to Glu; Mut) had little effect (Figures S1A and 2B–2D), suggesting that the function of NAT10 in promoting ESCA growth depends on its enzyme activity. In addition, wound healing and Transwell assays demonstrated that overexpression of WT NAT10, but not its catalytic mutant, can significantly promote the migration and invasion of ESCA cells (Figures 2E–2H). Furthermore, WT NAT10 significantly reduced cellular apoptosis of ESCA cells, and consistently, the NAT10 mutant showed little effect (Figures 2I and 2J). Taken together, these data support the essential functions of NAT10 and ac4C modification in promoting the progression of ESCA *in vitro*.

To investigate the role of NAT10 in ESCA progression *in vivo*, we established the epithelial tissue-specific *Nat10* conditional knockin (cKI; *Keratin14-CreER*; *Nat10* KI) mouse model (Figure 2K). We then induced ESCA tumorigenesis *in vivo* by adding 4-nitroquinoline-1-oxide (4-NQO) to the drinking water of 2-month-old mice for 16 weeks and then replaced it with normal water for 4 weeks (Figure 2L). After that, we used tamoxifen to induce the activation of *Nat10* transgene expression to study the roles of *Nat10* KI in ESCA progression (Figure 2L). Our data revealed that cKI of *Nat10* can significantly promote ESCA progression *in vivo*, as demonstrated by the enlarged esophagus and significant increases of the lesion areas and ESCA numbers (Figures 2M–2Q). Immunohistochemistry (IHC) staining revealed that the tumors in the esophagus of *Nat10* cKI mice showed higher expression of NAT10 and elevated levels of proliferation marker Ki67 (Figures 2R–2U), suggesting that *Nat10* cKI leads to ESCA with higher proliferation capacity. Overall, our data from the *in vitro* cell culture model and *in vivo Nat10* KI mice pro-

vided strong evidence supporting the important oncogenic function of NAT10 and its catalyzed ac4C RNA modifications in ESCA progression.

NAT10 inhibition impairs tumorigenesis of ESCA *in vitro* and in xenograft mouse model

To further explore the effect of NAT10 on ESCA progression, we knocked out NAT10 by CRISPR-Cas9 technique in two NAT10 high-expressing esophageal squamous cell carcinoma (ESCC) cells, TE9 and ECA109 (single guide GFP [sgGFP], sgNAT10-1, sgNAT10-2) (Figure 3A). Our results showed that knockout of NAT10 significantly inhibited the proliferation (Figure 3B) and colony-formation (Figures 3C and 3D) abilities in both TE9 and ECA109 cells. In addition, NAT10 knockout cells had significantly decreased migration and invasion capacities compared with the control sgGFP cells (Figures 3E–3H). Meanwhile, we examined the apoptosis level of NAT10 knockout and control ESCC cells by flow cytometry and found that NAT10 knockout increased the apoptosis levels in both TE9 and ECA109 cells (Figures 3I and 3J). We further used a xenograft mouse model to investigate the effect of NAT10 in ESCC progression *in vivo*. The results revealed that knockout of NAT10 significantly inhibited the tumorigenic ability of ESCC cells in xenograft mice (Figures 3K–3M). We then performed IHC staining and revealed that NAT10 and Ki67 levels in the tumors of the knockout group were significantly lower than the control group (Figures 3N–3Q), suggesting that NAT10 is essential for ESCC proliferation and growth *in vivo*. Similarly, depletion of NAT10 also significantly inhibited esophageal adenocarcinoma (EAC) progression *in vitro* and in xenograft mouse model (Figure S2). Overall, these data demonstrate the essential function of NAT10 in regulating the oncogenic progression in both ESCC and EAC cells.

Conditional knockout (cKO) of *Nat10* inhibits ESCA progression *in vivo*

To explore the physiological function of NAT10 in the development of ESCA *in vivo*, we generated the epithelial tissue-specific *Nat10* cKO (*Keratin14-CreER*; *Nat10 flox/flox*) mouse model (Figure 4A). After inducing ESCA formation with 4NQO, tamoxifen was applied to induce *Nat10* KO (cKO) to study the effect of *Nat10* on ESCA progression *in vivo* (Figure 4B). Our data revealed that *Nat10* cKO mice showed smaller esophagus enlargement and a significant decrease of lesion areas and ESCA numbers compared with the control mice (Control) (Figures 4C–4G). Moreover, IHC analysis uncovered that the ESCA tissues in *Nat10* KO mice showed reduced expression of NAT10 and a decreased level of proliferation marker Ki67

(G and H) Representative images (G) and quantitative analysis (H) of Transwell invasion in NC, WT, and MUT ESCA cells. Scale bar, 200 μm.

(I and J) Representative images (I) and quantitative analysis (J) of apoptosis in NC, WT, and MUT ESCA cells.

(K and L) The process of *Nat10* cKI and control mouse construction and treatment.

(M and N) Overview image (M) and lesion area quantification (N) in *Nat10* cKI and control mice.

(O) Representative image of H&E staining with esophagus tissues in *Nat10* cKI and control mice. Scale bar, 200 μm.

(P and Q) Dysplasia number (P) and ESCA number (Q) in esophagus tissues of *Nat10* cKI and control mice.

(R and S) Representative images (R) and H-score quantifications (S) of NAT10 IHC staining with esophagus tissues in *Nat10* cKI and control mice. Scale bar, 200 μm.

(T and U) Representative images (T) and H-score quantifications (U) of Ki67 IHC staining with esophagus tissues in *Nat10* cKI and control mice. Scale bar, 200 μm.

For histograms, each point represents an independent experiment, and the data are shown as the mean ± SD with p values labeled on individual panels. p values were calculated by two-tailed unpaired Student's t test.
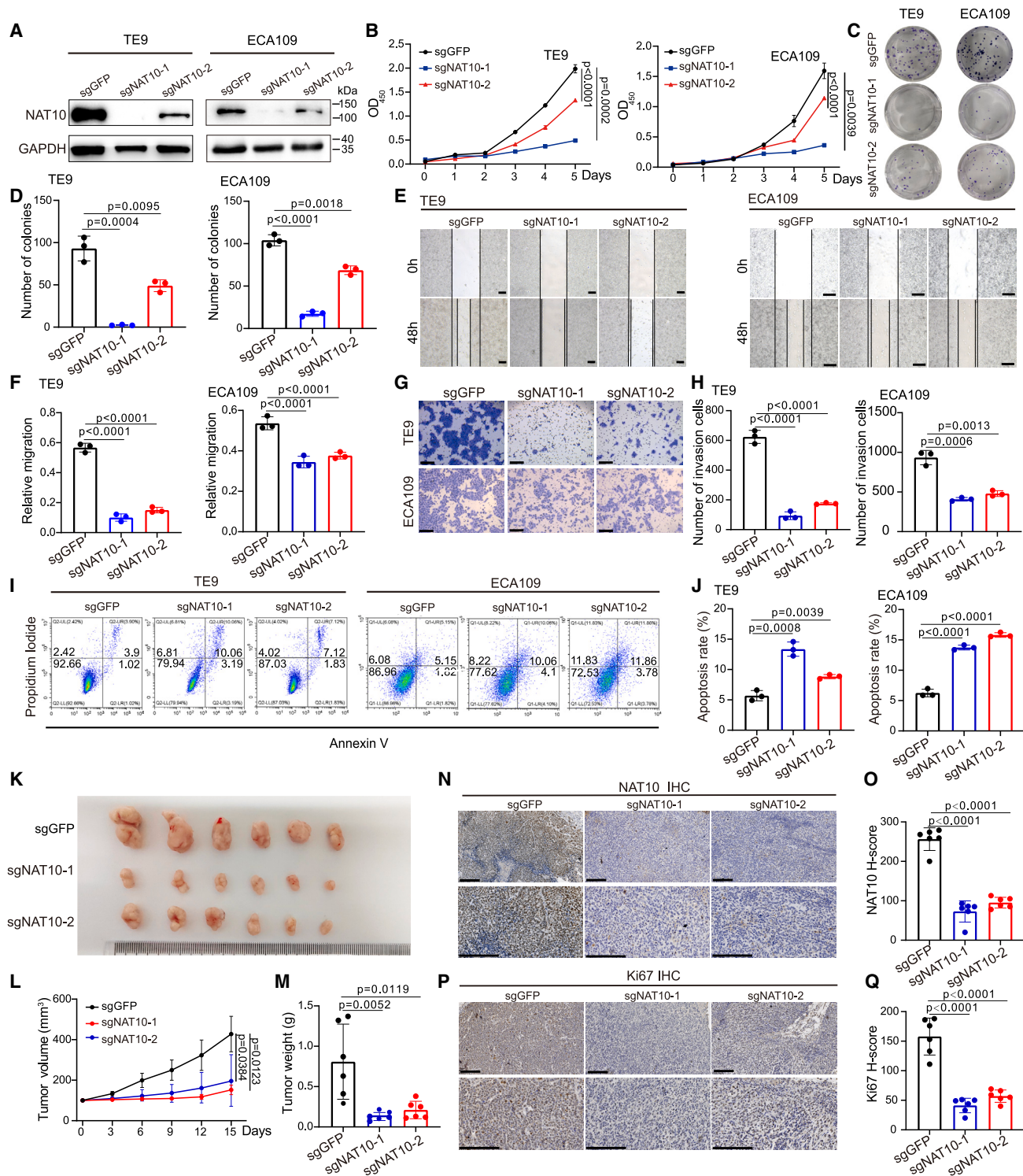
Figure 3. Inhibition of NAT10 impairs ESCC progression *in vitro* and *in vivo*

(A) Western blot of NAT10 in NAT10 KO and control ESCC cells.

(B) CCK8 assay of cell proliferation in NAT10 KO and control ESCC cells (n = 3).

(C and D) Representative images (C) and quantitative analysis (D) of colony formation in NAT10 KO and control ESCC cells.

(E and F) Representative images (E) and quantitative analysis (F) of wound healing in NAT10 KO and control ESCC cells. Scale bar, 200 μm.

(G and H) Representative images (G) and quantitative analysis (H) of Transwell invasion in NAT10 KO and control ESCC cells. Scale bar, 200 μm.

(legend continued on next page)

(Figures 4H–4K), which suggests that the cKO of *Nat10* decreased ESCA proliferation and progression *in vivo*. Taken together, data from our gain-of-function and loss-of-function studies using ESCA cells, xenograft mouse models, and ESCA progression models with the *Nat10* cKI and cKO mice provided strong evidence supporting the critical physiological functions of NAT10 in promoting ESCA progression *in vitro* and *in vivo*.

Chemical inhibition of ESCA progression with NAT10 inhibitor remodelin

Our above data uncovered that NAT10 could be a promising therapeutic target for ESCA, so we further developed therapeutic strategies by targeting NAT10 in ESCA. Remodelin is an effective small-molecule inhibitor of NAT10 that can specifically reduce the intracellular NAT10 level[25]; we therefore evaluated the therapeutic effect of remodelin on ESCA. Two ESCA cells (TE9 and ECA109) and two control cells (HEEC and Het-1A) were tested for their sensitivities to remodelin. Our data revealed that the TE9 and ECA109 ESCA cells showed higher expression of NAT10 and were more resistant to remodelin treatment (Figures S3A and S3B). We further revealed that remodelin treatment reduced the protein level of NAT10 and inhibited ESCA cell proliferation in a dose-dependent manner (Figures 4L and 4M). In addition, remodelin treatment significantly reduced colony-formation, migration, and invasion capacities in both TE9 and ECA109 ESCA cells (Figures 4N–4Q and S4). Moreover, remodelin treatment can significantly increase the apoptosis of both TE9 and ECA109 ESCA cells (Figures 4R and 4S), which is consistent with the reduced proliferation phenotype. Using the ESCA xenograft model, we further revealed that remodelin treatment significantly inhibited the growth of ESCA cells and decreased the expression levels of NAT10 and Ki67 *in vivo* (Figures 4T–4Z). These results supported that NAT10 is a promising therapeutic target in ESCA and that its inhibitor remodelin can effectively block ESCA progression *in vitro* and *in vivo*.

NAT10 catalyzes tRNA ac4C modifications, stabilizes tRNA expression, and promotes mRNA translation

To investigate the mechanisms of NAT10 in promoting ESCA progression, we performed ac4C RNA immunoprecipitation sequencing (ac4C-RIP-seq) using the sgNAT10 and the control ESCA cells. Our ac4C-RIP-seq uncovered that NAT10 catalyzes the ac4C modifications on a group of tRNAs and that KO of NAT10 leads to reduced ac4C modification levels and decreased expression of a majority of the ac4C modified tRNAs (Figures 5A and 5B). On the other hand, overexpression of NAT10 increased the expression of ac4C-modified tRNAs (Figure S1A). Given that tRNAs are essential modulators for mRNA translation, we further investigated the role of NAT10 in the regulation of mRNA translation. Our puromycin intake assay revealed

that depletion of NAT10 reduces the new protein synthesis rate (Figure 5C) and that overexpression of NAT10 increases new protein synthesis in ESCA cells (Figure S1B). Overall, these data suggest that NAT10-mediated ac4C tRNA modifications are essential for optimal mRNA translation.

We further performed a rescue experiment to support the essential function of tRNA in the regulation of NAT10's function in ESCA progression by overexpressing ac4C-target tRNAs (Gly-CCC and Lys-CTT) in NAT10-depleted ESCA cells. Our data revealed that overexpression of tRNA Gly-CCC or Lys-CTT can modestly increase proliferation, migration, and invasion of NAT10-depleted ESCA cells; importantly, overexpression of both Gly-CCC and Lys-CTT can further rescue the cancer progression phenotypes of NAT10-depleted ESCA cells (Figure S5). Overall, these data further support that ac4C-modified tRNAs contribute to the NAT10-mediated cancer progression phenotypes in ESCA cells.

To identify the downstream targets of NAT10, we performed polyribosome-bound mRNA sequencing (polyribosome-seq) to profile the mRNA translation efficiencies in sgNAT10 and control ESCA cells (Figure 5D; Table S1). We found that mRNAs with decreased translation efficiencies upon NAT10 depletion have higher numbers of codons decoded by the NAT10-regulated tRNAs (Figure 5E), suggesting that NAT10 may affect the translation of certain oncogenes in a codon-dependent mechanism. We next performed Gene Ontology (GO) and KEGG enrichment analyses and identified 10 genes that are commonly presented in the top 5 pathways found in both GO and KEGG analyses (Figures 5F–5H). Codon composition analysis revealed that EGFR contains the highest frequency of NAT10-regulated tRNA-decoded codons (Figure 5I, Table S2). In addition, our results showed that NAT10 KO decreases translation efficiency of EGFR mRNA and reduces the EGFR protein in ESCA cells (Figures 5J and 5K). Moreover, IHC staining using ESCA samples from the *Nat10* cKO and cKI mice revealed that the expression of EGFR is decreased in *Nat10* cKO and up-regulated in *Nat10* cKI ESCA samples (Figures 5L–5O). Taken together, these data suggest that EGFR could be an essential target of NAT10 in ESCA.

EGFR overexpression rescues oncogenic progression in NAT10-depleted ESCA cells

EGFR plays crucial functions in promoting ESCA progression and is an important diagnostic marker and therapeutic target in ESCA.[30,31] To evaluate the role of EGFR in NAT10-driven ESCA progression, we performed EGFR overexpression in NAT10-depleted ESCA cells. We found that overexpression of EGFR can partially rescue the impaired proliferation and colony-formation capacities of NAT10 KO TE9 and ECA109 ESCA cells (Figures 6A–6D). In addition, the migratory and invasive capacities of the NAT10-depleted ESCA cells are also partially

---

(I and J) Representative images (I) and quantitative analysis (J) of apoptosis in NAT10 KO and control ESCC cells.

(K) Overview of tumors in xenograft mice model subcutaneously implanted with NAT10 KO and control TE9 cells.

(L and M) Growth curves (n = 6) and weight of tumor in xenograft mice model.

(N–Q) Representative images and the quantitative H-scores of NAT10 (N and O) and Ki67 (P and Q) IHC staining of tumors obtained from the xenograft mice model. Scale bar, 200 μm.

For histograms, each point represents an independent experiment, and data are shown as mean ± SD with p values labeled on individual panels. p values were calculated by two-tailed unpaired Student's t test.
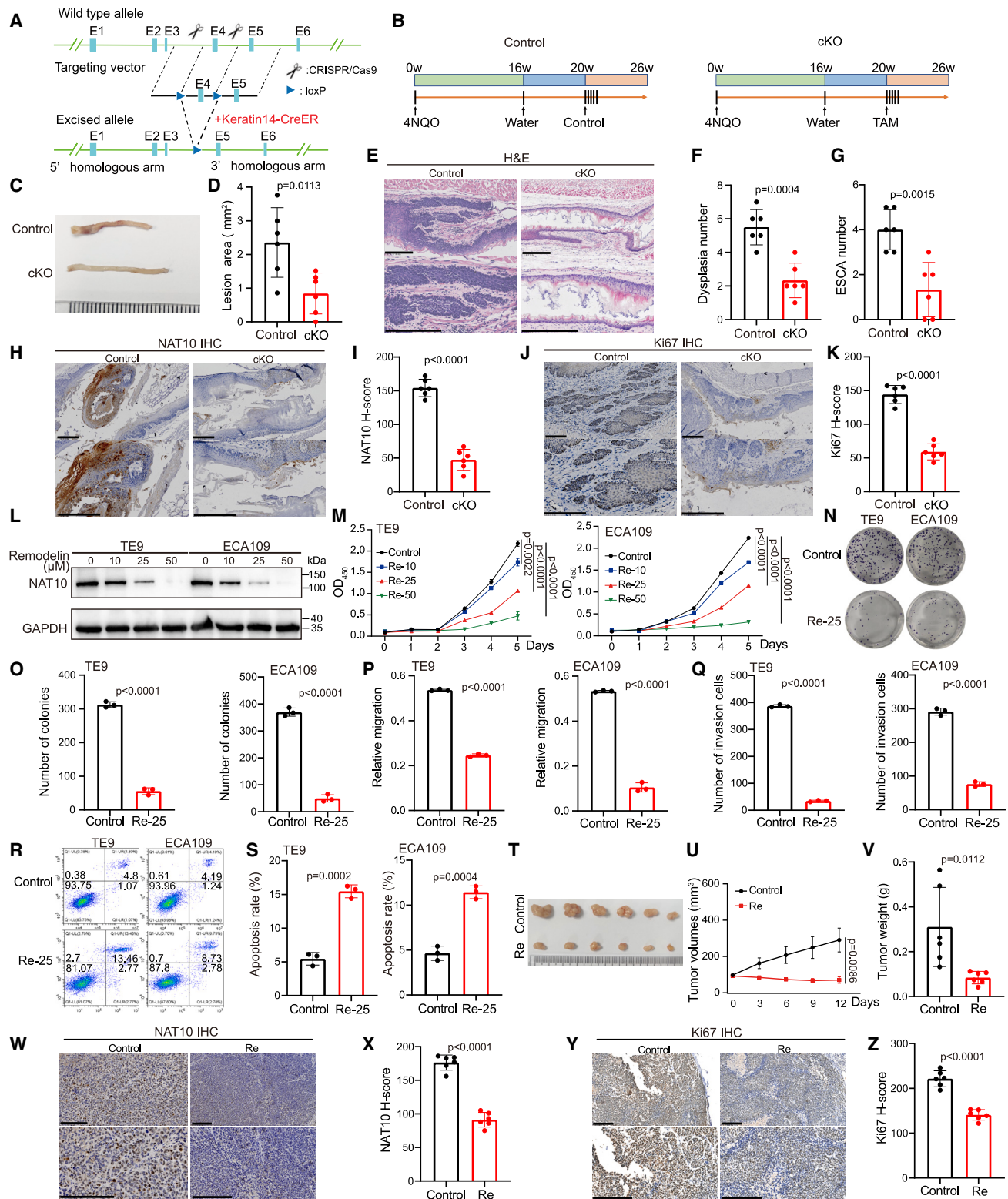
Figure 4. cKO and chemical inhibition of *Nat10* inhibit ESCA progression *in vitro* and *in vivo*

(A and B) The process of *Nat10* cKO and control mouse construction and treatment.

(C and D) Overview (C) and lesion area quantification (D) in *Nat10* cKO and control mice.

(E) Representative image of H&E staining with esophageal tissues in *Nat10* cKO and control mice. Scale bar, 200 μm.

(legend continued on next page)

restored by forced expression of EGFR (Figures 6E–6H). Moreover, EGFR overexpression can also reduce the number of apoptotic cells caused by NAT10 KO (Figures 6I and 6J). Taken together, our data demonstrated that EGFR is a critical downstream target of NAT10 that facilitates NAT10's oncogenic functions in promoting ESCA progression.

NAT10 promotes gefitinib resistance in ESCA

Gefitinib, a small-molecule inhibitor of EGFR, can improve the survival rate of patients with advanced stage ESCA and is a promising agent for second-line treatment of advanced ESCA, while relatively low response rate and drug resistance hinder its wide clinical application.[6,32] To explore the clinical relevance of the NAT10-ac4C-tRNA-EGFR oncogenic axis, we investigated the functions of NAT10 in the regulation of gefitinib efficacy in ESCA. Our data showed that gefitinib treatment inhibits ESCA cell proliferation and colony formation, while overexpression of NAT10 can partially restore the proliferation and colony-formation abilities of gefitinib-treated ESCA cells (Figures 6K–6M). Further analysis revealed that overexpression of NAT10 increases the IC50 of gefitinib (Figures S6A and S6B), while depletion of NAT10 leads to a decreased IC50 of gefitinib (Figures S6C and S6D), suggesting that NAT10 promotes the resistance to gefitinib treatment in ESCA cells. In addition, the effect of gefitinib treatment on cell migration and invasion can also be rescued by NAT10 overexpression (Figures 6N–6Q). Furthermore, NAT10 overexpression can reduce the apoptosis of ESCA cells caused by gefitinib treatment (Figures 6R and 6S). Overall, these data demonstrated that NAT10 overexpression can rescue the cancer progression phenotypes caused by gefitinib treatment, supporting that NAT10 promotes gefitinib resistance in ESCA.

NAT10 depletion and gefitinib treatment synergistically inhibit ESCA progression

We further explored whether targeting NAT10 combined with gefitinib can improve the treatment efficacy in ESCA. Our data showed that gefitinib treatment can further inhibit the cell proliferation and colony-formation capacities of NAT10 KO ESCC cells (Figures 7A–7C). In addition, the combination of gefitinib treatment and NAT10 KO synergistically inhibits the migration and invasion of both TE9 and ECA109 ESCC cells (Figures 7D and 7E). Moreover, under gefitinib treatment, the NAT10 KO TE9 and ECA109 ESCC cells showed higher apoptosis rates than the control cells (Figures 7F and 7G). We further investigated the efficacy of NAT10 KO on gefitinib in vivo. Our data showed that, in the ESCA xenograft model, gefitinib treatment significantly inhibited tumor growth, and the combination of gefitinib treatment and NAT10 KO further inhibited ESCC growth in vivo (Figures 7H–7J). An IHC assay also demonstrated the synergistical effect of combination therapy in the inhibition of ESCC proliferation, as shown by the decreased expression of proliferation marker Ki67 (Figures 7K–7P). Similarly, we also uncovered the synergistical effect of gefitinib and remodelin combination treatment in inhibiting the proliferation and invasion of OE19 and OE33 EAC cells (Figures S7). These results uncovered that NAT10 depletion and gefitinib treatment synergistically inhibit ESCA progression in vitro and in vivo, providing the molecular basis for development of novel therapeutic strategies for ESCA treatment.

DISCUSSION

ESCA is a deadly malignancy, and the treatment options for patients with advanced ESCA remain limited. Better understanding of the ESCA pathogenic mechanisms and identification of novel therapeutic targets are urgently needed for development of effective treatment strategies for patients with ESCA. In this study, we revealed that NAT10, the only enzyme known to catalyze ac4C RNA modification, is up-regulated in ESCA samples and is associated with poor prognosis of patients with ESCA. Using ESCA clinical samples, cell lines, xenograft mouse models, Nat10 cKI and cKO mouse ESCA models, and chemical inhibition approaches, we demonstrated the crucial physiological function of NAT10 in promoting ESCA progression in vitro and in vivo, suggesting that NAT10 is an important therapeutic target in ESCA.

Our ac4C RIP-seq revealed that NAT10 catalyzes the ac4C modifications on a subset of tRNAs and that KO of NAT10 caused decreased expression of ac4C-modified tRNAs and reduced translation efficiencies of mRNAs in an ac4C tRNA-associated codon-dependent manner. Emerging studies have shown that mis-regulated tRNA modifications cause many human diseases including human cancers.[33,34] Our previous studies revealed that N[7]-methylguanosine (m[7]G) tRNA

(F and G) Dysplasia number (F) and ESCA number (G) in esophageal tissues of Nat10 cKO and control mice.
(H and I) Representative images (H) and H-score quantifications (I) of NAT10 IHC staining of esophageal tissues in Nat10 cKO and control mice. Scale bar, 200 μm.
(J and K) Representative images (J) and H-score quantification (K) of Ki67 IHC staining of esophageal tissues in Nat10 cKO and control mice. Scale bar, 200 μm.
(L) Western blot analysis of NAT10 in ESCA cells after treatment with different concentrations of remodelin (Re stands for remodelin treatment, and the number after it represents the concentration of the treatment, μM).
(M) CCK8 assay of ESCA cells treated by different concentrations of remodelin (Re-50: 50 μM; Re-25: 25 μM; Re-10: 10 μM) or DMSO (control) (n = 3).
(N and O) Representative images (N) and quantitative analysis (O) of colony formation in ESCA cells treated by remodelin (25 μM) or DMSO (control).
(P) Quantitative analysis of wound healing with ESCA cells treated by remodelin (25 μM) or DMSO (control).
(Q) Quantitative analysis of Transwell invasion with ESCA cells treated by remodelin (25 μM) or DMSO (control).
(R and S) Representative images (R) and quantitative analysis (S) of apoptosis in ESCA cells treated by remodelin (25 μM) or DMSO (control).
(T) Overview of tumors in xenograft mice model subcutaneously implanted with TE9 cells and then treated with remodelin or DMSO (control).
(U and V) Growth curves (U) (n = 6) and weight (V) of tumor in xenograft mice model with remodelin or DMSO (control).
(W and X) Representative images (W) and H-score quantification (X) of NAT10 IHC staining in xenograft mice model.
(Y and Z) Representative images (Y) and H-score quantification (Z) of Ki67 IHC staining in xenograft mice model.
For histograms, each point represents an independent experiment, and the data are shown as the mean ± SD with p values labeled on individual panels. p values were calculated by two-tailed unpaired Student's t test.
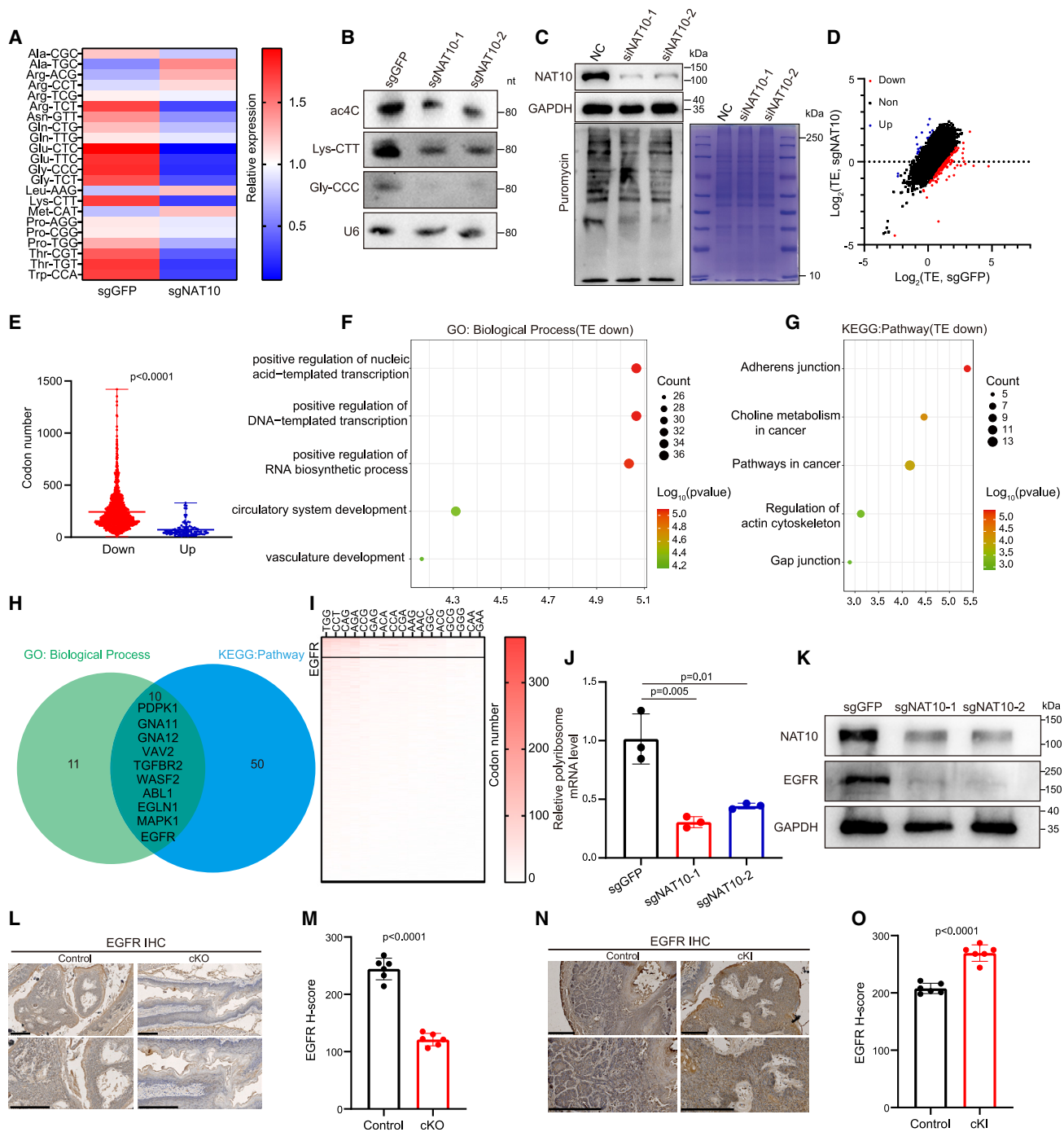
Figure 5. NAT10 catalyzes tRNA ac4C modifications, stabilizes tRNA expression, and promotes mRNA translation

(A) Comparative abundance of tRNAs with ac4C modifications in sgGFP and sgNAT10 obtained by ac4C-RIP-seq analysis.

(B) Northern blot and northwestern blot analysis of tRNA with ac4C modification, Lys-CTT, and Gly-CCC level in sgGFP and NAT10 KO TE9 cells. ac4C level was detected by northwestern blot with anti-ac4C antibody. Levels of Lys-CTT, Gly-CCC, and U6 were detected by northern blot with indicated probes.

(C) Puromycin analysis of sgGFP and NAT10 KO TE9 cells. SDS-PAGE analysis was used as loading control.

(D) Polyribosome-seq profiling the changes of translation efficiencies (TEs) in NAT10 KO TE9 cells. Up, up-regulated; Non, non-regulated; Down, down-regulated.

(E) Comparison of the number of codons decoded by reduced ac4C tRNAs on TE down-regulated and up-regulated transcripts.

(F and G) Gene Ontology analysis (F) and pathway analysis (G) using the TE-down genes.

(H) Venn graph of overlapping genes in Gene Ontology analysis and pathway analysis.

(I) Number of codons decoded by reduced ac4C tRNAs with all gene transcripts in polyribosome-seq.

(legend continued on next page)

modifications catalyzed by METTL1 promote the development of various tumors including ESCA.[12,35,36] Here, we uncovered that NAT10-mediated ac4C tRNA modifications can preferentially promote the translation of mRNAs with higher ac4C tRNA-decoded codons. These data provided insights into post-transcriptional gene expression regulation mechanisms mediated by tRNA modifications and mRNA codon composition.

Translation profiling identified EGFR as an essential target of NAT10 in the regulation of ESCA progression. EGFR is an important oncogenic driving factor in diverse cancers including lung cancer and ESCA.[6,37,38] The hyperactivation of EGFR could be caused by multiple mechanisms.[39] It was reported that genomic amplifications and epigenetic modifications can lead to the over-expression of EGFR mRNA in cancers.[39,40] In addition, genetic activating mutations in the EGFR gene could result in ligand-independent constitutive activation of EGFR activity.[41–43] Here, we showed that NAT10-mediated ac4C tRNA expression promotes the translation efficiency of EGFR mRNA, uncovering an additional layer of the molecular mechanism underlying EGFR hyperactivation in cancers at the mRNA translation level.

The EGFR small-molecule inhibitor gefitinib is a widely used drug for treatment of cancers with EGFR overactivation and is for second-line treatment of advanced ESCAs.[6,32] Our data showed that NAT10 overexpression can partially rescue the impaired cancer progression phenotypes upon gefitinib treatment. On the other hand, the combination of NAT10 depletion and gefitinib treatment synergistically inhibits ESCA progression *in vitro* and *in vivo*. The low response rate and resistance of gefitinib hinder its wide clinical application, and our study provides a theoretical basis for the development of novel therapeutic strategies to improve gefitinib sensitivity and efficacy for cancer therapy.

In conclusion, we demonstrated the crucial physiological functions of NAT10-mediated ac4C tRNA modification in regulating ESCA progression. Our data uncovered the molecular mechanisms underlying ESCA progression and provided insights for the development of effective cancer therapeutic strategies through the combination of gefitinib and NAT10-targeted agents.

Limitations of the study

The limitations of this study include the following: first, here we demonstrate that ac4C-modified tRNAs are essential targets of NAT10 that promote translation and ESCA progression; however, it has been reported that NAT10 could regulate the ac4C modification on mRNAs and rRNAs, which could also participate in NAT10's function in ESCA. Second, although the expression levels of NAT10 in tumor tissues are significantly higher than healthy tissues, and the ESCA cells are more sensitive to NAT10 inhibition, the potential side effects of targeting NAT10 need to be considered. Therefore, finding the therapeutic win-

dow that can maximize the killing of the ESCA cells but minimize the side effects on healthy cells will be essential for the clinical application of NAT10 inhibitors for cancer treatment. Finally, though previous clinical trials revealed that gefitinib treatment could show an overall survival benefit in a subgroup of patients with advanced ESCA, currently its clinical application for treatment of ESCA has not been approved. Further studies are needed to explore the correlation between NAT10 expression and gefitinib resistance in patients and to develop effective combination therapeutic strategies for cancer treatment.

STAR★METHODS

Detailed methods are provided in the online version of this paper and include the following:

- KEY RESOURCES TABLE
- RESOURCE AVAILABILITY
  ○ Lead contact
  ○ Materials availability
  ○ Data and code availability
- EXPERIMENTAL MODEL AND SUBJECT PARTICIPANT DETAILS
  ○ Patient samples
  ○ Xenograft mouse model
  ○ Generation of *Nat10* conditional knockout and conditional knockin mice
- METHOD DETAILS
  ○ Immunohistochemistry (IHC) staining
  ○ Cell culture
  ○ Knockout and overexpression of NAT10 in ESCA cells
  ○ RNA extraction and qRT-PCR
  ○ Western blot, northwestern blot, and northern blot
  ○ Colony-formation, cell proliferation assays
  ○ Cell apoptosis assays
  ○ Puromycin intake assay
  ○ ac4C RNA immunoprecipitation sequencing (ac4C-RIP-seq)
  ○ Analysis of ac4C-RIP-seq
  ○ Polyribosome-bound mRNAs sequencing (polyribosome-seq)
  ○ Gene pathway enrichment analysis
  ○ Hematoxylin and eosin stain (H&E) staining
  ○ Inhibitor treatment *in vivo* and *in vitro*
- QUANTIFICATION AND STATISTICAL ANALYSIS

SUPPLEMENTAL INFORMATION

Supplemental information can be found online at https://doi.org/10.1016/j.celrep.2023.112810.

(J) Polyribosome-associated mRNA-qPCR assay of the EGFR in sgGFP and NAT10 KO TE9 cells.

(K) Western blot analysis of NAT10 and EGFR levels in sgGFP and NAT10 KO TE9 cells.

(L and M) Representative images (L) and H-score quantification (M) of EGFR IHC staining with esophagus tissues in *Nat10* cKO and control mice. Scale bar, 200 μm.

(N and O) Representative images (N) and H-score quantification (O) of EGFR IHC staining with esophagus tissues in *Nat10* cKI and control mice. Scale bar, 200 μm.

For histograms, each point represents an independent experiment, and the data are shown as the mean ± SD with p values labeled on individual panels. p values were calculated by two-tailed unpaired Student's t test.
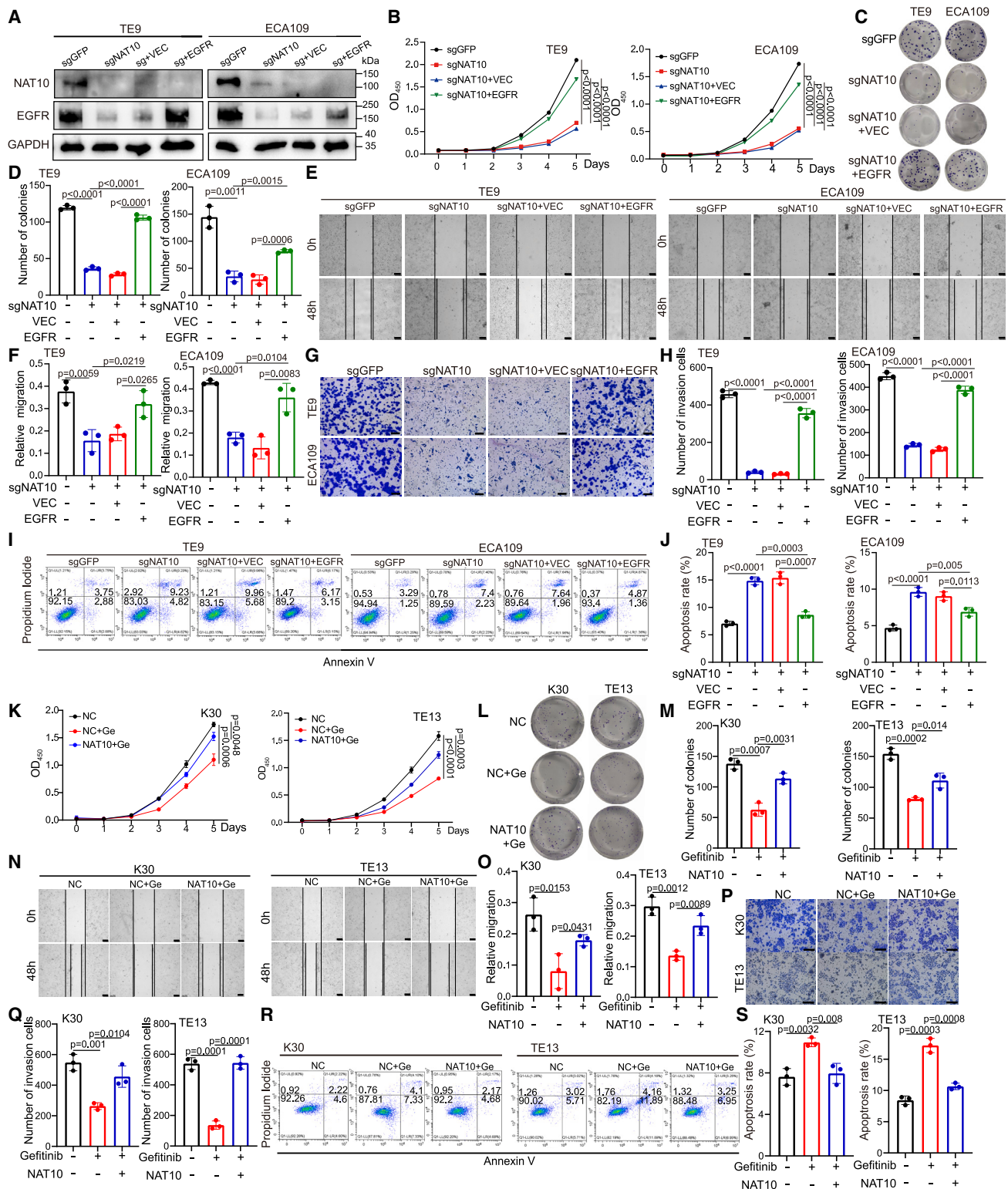
Figure 6. EGFR is a key downstream target of NAT10 that mediates its function in gefitinib resistance

(A) The levels of NAT10 and EGFR in NAT10 KO cells with or without EGFR overexpression.

(B) CCK8 assay of growth in NAT10 KO cells with or without EGFR overexpression (n = 3).

(C and D) Representative images (C) and quantitative analysis (D) of colony formation in NAT10 KO cells with or without EGFR overexpression.

(legend continued on next page)

AUTHOR CONTRIBUTIONS

W.W., J.C., and S.L. designed the protocol of this study. W.W., S.Z., H.H., and X.W. performed most of the experiments. S.Z. provided the clinical sample tissues. S.Z., Z.W., C.Y., L.W., J.M., S.G., J.W., and L.L. helped with part of the experiment. W.W., J.C., and S.L. wrote the manuscript with input from all other authors.

DECLARATION OF INTERESTS

The authors declare no competing interests.

INCLUSION AND DIVERSITY

We support inclusive, diverse, and equitable conduct of research.

REFERENCES

1. Uhlenhopp, D.J., Then, E.O., Sunkara, T., and Gaduputi, V. (2020). Epidemiology of esophageal cancer: update in global trends, etiology and risk factors. Clin. J. Gastroenterol. *13*, 1010–1021. https://doi.org/10.1007/s12328-020-01237-x.

2. Ajani, J., D'Amico, T.A., Hayman, J.A., Meropol, N.J., and Minsky, B.; National Comprehensive Cancer Network (2003). Esophageal cancer. Clinical practice guidelines in oncology. J. Natl. Compr. Canc. Netw. *1*, 14–27. https://doi.org/10.6004/jnccn.2003.0004.

3. Sakaeda, T., Yamamori, M., Kuwahara, A., and Nishiguchi, K. (2009). Pharmacokinetics and pharmacogenomics in esophageal cancer chemoradiotherapy. Adv. Drug Deliv. Rev. *61*, 388–401. https://doi.org/10.1016/j.addr.2008.10.005.

4. Rogers, J.E., Sewastjanow-Silva, M., Waters, R.E., and Ajani, J.A. (2022). Esophageal cancer: emerging therapeutics. Expert Opin. Ther. Targets *26*, 107–117. https://doi.org/10.1080/14728222.2022.2036718.

5. Zubair, T., and Bandyopadhyay, D. (2023). Small Molecule EGFR Inhibitors as Anti-Cancer Agents: Discovery, Mechanisms of Action, and Opportunities. Int. J. Mol. Sci. *24*, 2651. https://doi.org/10.3390/ijms24032651.

6. Petty, R.D., Dahle-Smith, A., Stevenson, D.A.J., Osborne, A., Massie, D., Clark, C., Murray, G.I., Dutton, S.J., Roberts, C., Chong, I.Y., et al. (2017). Gefitinib and EGFR Gene Copy Number Aberrations in Esophageal Cancer. J. Clin. Oncol. *35*, 2279–2287. https://doi.org/10.1200/JCO.2016.70.3934.

7. Meemanage, M., Spender, L.C., Collinson, D., Iannetta, J., Challapalli, P., Turbitt, J., Clark, C., Baxter, M., Murray, G., Walsh, S., et al. (2021). Interactions between anti-EGFR therapies and cytotoxic chemotherapy in oesophageal squamous cell carcinoma: why clinical trials might have failed and how they could succeed. Cancer Chemother. Pharmacol. *87*, 361–377. https://doi.org/10.1007/s00280-020-04187-w.

8. Xu, Y., Xie, Z., Shi, Y., Zhang, M., Pan, J., Li, Y., and Lu, H. (2016). Gefitinib single drug in treatment of advanced esophageal cancer. J. Cancer Res. Ther. *12*, C295-C297. https://doi.org/10.4103/0973-1482.200760.

9. Huang, F.L., and Yu, S.J. (2018). Esophageal cancer: Risk factors, genetic association, and treatment. Asian J. Surg. *41*, 210–215. https://doi.org/10.1016/j.asjsur.2016.10.005.

10. Kaz, A.M., and Grady, W.M. (2014). Epigenetic biomarkers in esophageal cancer. Cancer Lett. *342*, 193–199. https://doi.org/10.1016/j.canlet.2012.02.036.

11. Zhao, R., and Casson, A.G. (2008). Epigenetic aberrations and targeted epigenetic therapy of esophageal cancer. Curr. Cancer Drug Targets *8*, 509–521. https://doi.org/10.2174/156800908785699306.

12. Han, H., Yang, C., Ma, J., Zhang, S., Zheng, S., Ling, R., Sun, K., Guo, S., Huang, B., Liang, Y., et al. (2022). N(7)-methylguanosine tRNA modification promotes esophageal squamous cell carcinoma tumorigenesis via the RPTOR/ULK1/autophagy axis. Nat. Commun. *13*, 1478. https://doi.org/10.1038/s41467-022-29125-7.

13. Li, Y., Niu, C., Wang, N., Huang, X., Cao, S., Cui, S., Chen, T., Huo, X., and Zhou, R. (2022). The Role of m(6)A Modification and m(6)A Regulators in Esophageal Cancer. Cancers *14*, 5139. https://doi.org/10.3390/cancers14205139.

14. Han, H., Yang, C., Zhang, S., Cheng, M., Guo, S., Zhu, Y., Ma, J., Liang, Y., Wang, L., Zheng, S., et al. (2021). METTL3-mediated m(6)A mRNA modification promotes esophageal cancer initiation and progression via Notch signaling pathway. Mol. Ther. Nucleic Acids *26*, 333–346. https://doi.org/10.1016/j.omtn.2021.07.007.

15. Zhao, B.S., Roundtree, I.A., and He, C. (2017). Post-transcriptional gene regulation by mRNA modifications. Nat. Rev. Mol. Cell Biol. *18*, 31–42. https://doi.org/10.1038/nrm.2016.132.

16. Barbieri, I., and Kouzarides, T. (2020). Role of RNA modifications in cancer. Nat. Rev. Cancer *20*, 303–322. https://doi.org/10.1038/s41568-020-0253-2.

(E and F) Representative images (E) and quantitative analysis (F) of wound healing in NAT10 KO cells with or without EGFR overexpression. Scale bar, 200 μm.

(G and H) Representative images (G) and quantitative analysis (H) of Transwell invasion in NAT10 KO cells with or without EGFR overexpression. Scale bar, 200 μm.

(I and J) Representative images (I) and quantitative analysis (J) of apoptosis in NAT10 KO cells with or without EGFR overexpression.

(K) CCK8 analysis after treatment with gefitinib (Ge stands for gefitinib treatment, and the number after it represents the concentration of the treatment, μM) to the control and NAT10 overexpression groups (n = 3).

(L and M) Representative images (L) and quantitative analysis (M) of colony formation in NAT10 overexpression and control ESCA cells after treatment with gefitinib.

(N and O) Representative images (N) and quantitative analysis (O) of wound healing in NAT10 overexpression and control ESCA cells after treatment with gefitinib. Scale bar, 200 μm.

(P and Q) Representative images (P) and quantitative analysis (Q) of Transwell invasion in NAT10 overexpression and control ESCA cells after treatment with gefitinib. Scale bar, 200 μm.

(R and S) Representative images (R) and quantitative analysis (S) of apoptosis in NAT10 overexpression and control ESCA cells after treatment with gefitinib. For histograms, each point represents an independent experiment, and the data are shown as the mean ± SD with p values labeled on individual panels. p values were calculated by two-tailed unpaired Student's t test.
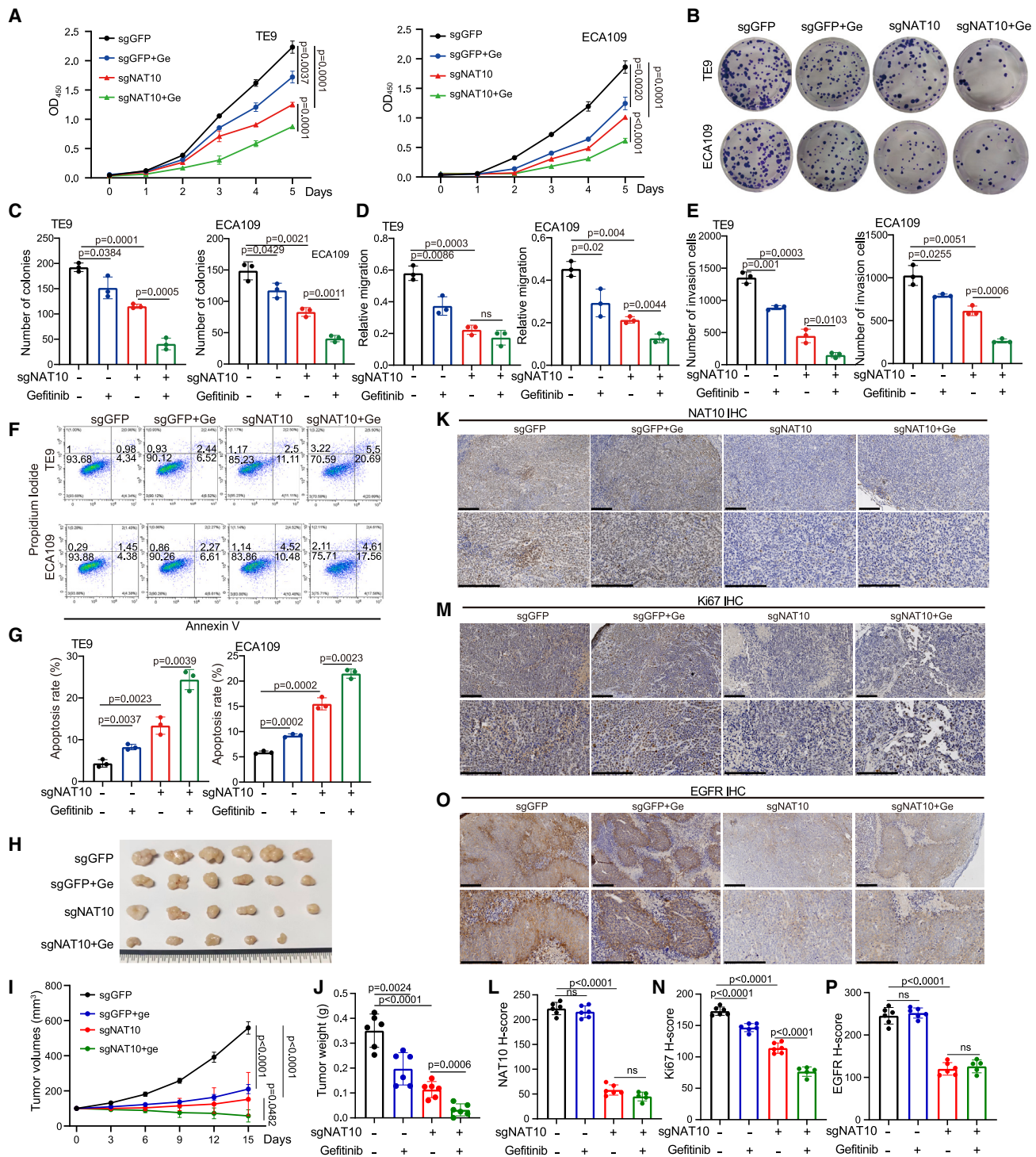
Figure 7. Combination of NAT10 depletion and gefitinib treatment synergistically inhibits ESCA progression

(A) CCK8 analysis in NAT10 KO and control ESCA cells after treatment with gefitinib (n = 3).

(B and C) Representative images (B) and quantitative analysis (C) of colony formation in NAT10 KO and control ESCA cells after treatment with gefitinib.

(D) Quantitative analysis of wound healing in NAT10 KO and control ESCA cells after treatment with gefitinib.

(E) Quantitative analysis of Transwell invasion in NAT10 KO and control ESCA cells after treatment with gefitinib.

(F and G) Representative images (F) and quantitative analysis (G) of apoptosis assay in NAT10 KO and control ESCA cells after treatment with gefitinib.

(H) Overview of tumors in xenograft mice model that were subcutaneously implanted with NAT10 KO and control ESCA cells after treatment of gefitinib.

(I and J) Growth curves (I) (n = 6) and weight (J) of tumor in xenograft mice model after treatment of gefitinib.

17. Peng, H., Chen, B., Wei, W., Guo, S., Han, H., Yang, C., Ma, J., Wang, L., Peng, S., Kuang, M., and Lin, S. (2022). N(6)-methyladenosine (m(6)A) in 18S rRNA promotes fatty acid metabolism and oncogenic transformation. Nat. Metab. *4*, 1041–1054. https://doi.org/10.1038/s42255-022-00622-9.

18. Lin, S., Choe, J., Du, P., Triboulet, R., and Gregory, R.I. (2016). The m(6)A Methyltransferase METTL3 Promotes Translation in Human Cancer Cells. Mol. Cell *62*, 335–345. https://doi.org/10.1016/j.molcel.2016.03.021.

19. Jin, G., Xu, M., Zou, M., and Duan, S. (2020). The Processing, Gene Regulation, Biological Functions, and Clinical Relevance of N4-Acetylcytidine on RNA: A Systematic Review. Molecular therapy. Nucleic acids *20*, 13–24. https://doi.org/10.1016/j.omtn.2020.01.037.

20. Sas-Chen, A., Thomas, J.M., Matzov, D., Taoka, M., Nance, K.D., Nir, R., Bryson, K.M., Shachar, R., Liman, G.L.S., Burkhart, B.W., et al. (2020). Dynamic RNA acetylation revealed by quantitative cross-evolutionary mapping. Nature *583*, 638–643. https://doi.org/10.1038/s41586-020-2418-2.

21. Tsai, K., Jaguva Vasudevan, A.A., Martinez Campos, C., Emery, A., Swanstrom, R., and Cullen, B.R. (2020). Acetylation of Cytidine Residues Boosts HIV-1 Gene Expression by Increasing Viral RNA Stability. Cell Host Microbe *28*, 306–312.e6. https://doi.org/10.1016/j.chom.2020.05.011.

22. Arango, D., Sturgill, D., Alhusaini, N., Dillman, A.A., Sweet, T.J., Hanson, G., Hosogane, M., Sinclair, W.R., Nanan, K.K., Mandler, M.D., et al. (2018). Acetylation of Cytidine in mRNA Promotes Translation Efficiency. Cell *175*, 1872–1886.e24. https://doi.org/10.1016/j.cell.2018.10.030.

23. Wang, G., Zhang, M., Zhang, Y., Xie, Y., Zou, J., Zhong, J., Zheng, Z., Zhou, X., Zheng, Y., Chen, B., and Liu, C. (2022). NAT10-mediated mRNA N4-acetylcytidine modification promotes bladder cancer progression. Clin. Transl. Med. *12*, e738. https://doi.org/10.1002/ctm2.738.

24. Zhang, Y., Jing, Y., Wang, Y., Tang, J., Zhu, X., Jin, W.L., Wang, Y., Yuan, W., Li, X., and Li, X. (2021). NAT10 promotes gastric cancer metastasis via N4-acetylated COL5A1. Signal Transduct. Target. Ther. *6*, 173. https://doi.org/10.1038/s41392-021-00489-4.

25. Larrieu, D., Britton, S., Demir, M., Rodriguez, R., and Jackson, S.P. (2014). Chemical inhibition of NAT10 corrects defects of laminopathic cells. Science *344*, 527–532. https://doi.org/10.1126/science.1252651.

26. Balmus, G., Larrieu, D., Barros, A.C., Collins, C., Abrudan, M., Demir, M., Geisler, N.J., Lelliott, C.J., White, J.K., Karp, N.A., et al. (2018). Targeting of NAT10 enhances healthspan in a mouse model of human accelerated aging syndrome. Nat. Commun. *9*, 1700. https://doi.org/10.1038/s41467-018-03770-3.

27. Chen, L., Wang, W.J., Liu, Q., Wu, Y.K., Wu, Y.W., Jiang, Y., Liao, X.Q., Huang, F., Li, Y., Shen, L., et al. (2022). NAT10-mediated N4-acetylcytidine modification is required for meiosis entry and progression in male germ cells. Nucleic Acids Res. *50*, 10896–10913. https://doi.org/10.1093/nar/gkac594.

28. Larrieu, D., Viré, E., Robson, S., Breusegem, S.Y., Kouzarides, T., and Jackson, S.P. (2018). Inhibition of the acetyltransferase NAT10 normalizes progeric and aging cells by rebalancing the Transportin-1 nuclear import pathway. Sci. Signal. *11*, eaar5401. https://doi.org/10.1126/scisignal.aar5401.

29. Liu, H.Y., Liu, Y.Y., Yang, F., Zhang, L., Zhang, F.L., Hu, X., Shao, Z.M., and Li, D.Q. (2020). Acetylation of MORC2 by NAT10 regulates cell-cycle checkpoint control and resistance to DNA-damaging chemotherapy and radiotherapy in breast cancer. Nucleic Acids Res. *48*, 3638–3656. https://doi.org/10.1093/nar/gkaa130.

30. Jiang, D., Li, X., Wang, H., Shi, Y., Xu, C., Lu, S., Huang, J., Xu, Y., Zeng, H., Su, J., et al. (2015). The prognostic value of EGFR overexpression and

31. amplification in Esophageal squamous cell Carcinoma. BMC Cancer *15*, 377. https://doi.org/10.1186/s12885-015-1393-8.

31. Bai, M., Wang, M., Deng, T., Bai, Y., Zang, K., Miao, Z., Gai, W., Xie, L., and Ba, Y. (2022). Safety and efficacy of anti-EGFR monoclonal antibody (SCT200) as second-line therapy in advanced esophageal squamous cell carcinoma. Cancer Biol. Med. *19*, 358–369. https://doi.org/10.20892/j.issn.2095-3941.2021.0388.

32. Janmaat, M.L., Gallegos-Ruiz, M.I., Rodriguez, J.A., Meijer, G.A., Vervenne, W.L., Richel, D.J., Van Groeningen, C., and Giaccone, G. (2006). Predictive factors for outcome in a phase II study of gefitinib in second-line treatment of advanced esophageal cancer patients. J. Clin. Oncol. *24*, 1612–1619. https://doi.org/10.1200/JCO.2005.03.4900.

33. Li, J., Zhu, W.Y., Yang, W.Q., Li, C.T., and Liu, R.J. (2021). The occurrence order and cross-talk of different tRNA modifications. Sci. China Life Sci. *64*, 1423–1436. https://doi.org/10.1007/s11427-020-1906-4.

34. Suzuki, T. (2021). The expanding world of tRNA modifications and their disease relevance. Nat. Rev. Mol. Cell Biol. *22*, 375–392. https://doi.org/10.1038/s41580-021-00342-0.

35. Ma, J., Han, H., Huang, Y., Yang, C., Zheng, S., Cai, T., Bi, J., Huang, X., Liu, R., Huang, L., et al. (2021). METTL1/WDR4-mediated m(7)G tRNA modifications and m(7)G codon usage promote mRNA translation and lung cancer progression. Mol. Ther. *29*, 3422–3435. https://doi.org/10.1016/j.ymthe.2021.08.005.

36. Dai, Z., Liu, H., Liao, J., Huang, C., Ren, X., Zhu, W., Zhu, S., Peng, B., Li, S., Lai, J., et al. (2021). N(7)-Methylguanosine tRNA modification enhances oncogenic mRNA translation and promotes intrahepatic cholangiocarcinoma progression. Mol. Cell *81*, 3339–3355.e8. https://doi.org/10.1016/j.molcel.2021.07.003.

37. Passaro, A., Jänne, P.A., Mok, T., and Peters, S. (2021). Overcoming therapy resistance in EGFR-mutant lung cancer. Nat. Cancer *2*, 377–391. https://doi.org/10.1038/s43018-021-00195-8.

38. Nicholson, R.I., Gee, J.M., and Harper, M.E. (2001). EGFR and cancer prognosis. Eur. J. Cancer *37* (Suppl 4), S9-S15. https://doi.org/10.1016/s0959-8049(01)00231-3.

39. Bethune, G., Bethune, D., Ridgway, N., and Xu, Z. (2010). Epidermal growth factor receptor (EGFR) in lung cancer: an overview and update. J. Thorac. Dis. *2*, 48–51.

40. al-Kasspooles, M., Moore, J.H., Orringer, M.B., and Beer, D.G. (1993). Amplification and over-expression of the EGFR and erbB-2 genes in human esophageal adenocarcinomas. Int. J. Cancer *54*, 213–219. https://doi.org/10.1002/ijc.2910540209.

41. Lynch, T.J., Bell, D.W., Sordella, R., Gurubhagavatula, S., Okimoto, R.A., Brannigan, B.W., Harris, P.L., Haserlat, S.M., Supko, J.G., Haluska, F.G., et al. (2004). Activating mutations in the epidermal growth factor receptor underlying responsiveness of non-small-cell lung cancer to gefitinib. N. Engl. J. Med. *350*, 2129–2139. https://doi.org/10.1056/NEJMoa040938.

42. Gazdar, A.F. (2009). Activating and resistance mutations of EGFR in non-small-cell lung cancer: role in clinical response to EGFR tyrosine kinase inhibitors. Oncogene *28* (Suppl 1), S24-S31. https://doi.org/10.1038/onc.2009.198.

43. Sudo, T., Mimori, K., Nagahara, H., Utsunomiya, T., Fujita, H., Tanaka, Y., Shirouzu, K., Inoue, H., and Mori, M. (2007). Identification of EGFR mutations in esophageal cancer. Eur. J. Surg. Oncol. *33*, 44–48. https://doi.org/10.1016/j.ejso.2006.10.034.

(K and L) Representative images (K) and H-score quantifications (L) of NAT10 IHC staining in xenograft tumors. Scale bar, 200 μm.

(M and N) Representative images (M) and H-score quantifications (N) of Ki67 IHC staining in xenograft tumors. Scale bar, 200 μm.

(O and P) Representative images (O) and H-score quantifications (P) of EGFR IHC staining in xenograft tumors. Scale bar, 200 μm.

For histograms, each point represents an independent experiment, and the data are shown as the mean ± SD with p values labeled on individual panels. p values were calculated by two-tailed unpaired Student's t test.

STAR★METHODS

KEY RESOURCES TABLE

REAGENT or RESOURCE	SOURCE	IDENTIFIER
Antibodies		
Anti-rabbit IgG HRP-linked Antibody	Cell signaling technology	Cat# 7074S; RRID: AB_2099233
Anti-mouse IgG HRP-linked Antibody	Cell signaling technology	Cat# 7076S; RRID: AB_330924
Rabbit polyclonal anti- CD31	Abcam	Cat#ab28364; RRID: AB_726362
Mouse monoclonal anti-puromycin	Millipore	Cat# MABE343; RRID: AB_2566826
Rabbit polyclonal anti-GAPDH	Proteintech	Cat# 10494-1-AP; RRID: AB_2263076
Rabbit monoclonal to N4-acetylcytidine	Abcam	Cat#ab252215; RRID: AB_2827750
Rabbit polyclonal anti-Ki67	Abcam	Cat# ab15580; RRID: AB_443209
Rabbit polyclonal anti-NAT10	Proteintech	Cat#13365-1-AP; RRID: AB_2148944
Rabbit polyclonal anti-EGFR	Proteintech	Cat# 18986-1-AP; RRID: AB_10596476
Biological samples		
Human ESCA tissues	The First Affiliated Hospital Sun Yat-sen University	N/A
Chemicals, peptides, and recombinant proteins		
ML-60218	TargetMol	CAS No: 577784-91-9
Remodelin	MCE	CAS No: 1622921-15-6
Gefitinib	sellect	CAS No: 184475-35-2
Deposited data		
Raw data of Polyribosome-seq	This study	GEO: GSE225131
Raw data of ac4C-RIP-seq	This study	GEO: GSE225131
Experimental models: Cell lines		
TE9	Gift from Lizu Wu lab	N/A
ECA109	Shanghai EK-Bioscience Biotechnology, China	CC-Y1150
TE13	Shanghai EK-Bioscience Biotechnology, China	CC-Y1515
KYSE-30	Shanghai EK-Bioscience Biotechnology, China	CC-Y1314
OE33	Hefei Wanwu Biotechnology, China	wanwu19322
OE19	Hefei Wanwu Biotechnology, China	wanwu19273
Het-1A	Nanjing shrbio, China	SHC8231
HEEC	Nanjing shrbio, China	SHC6723
293T	ATCC, USA	CRL-3216
Experimental models: Organisms/strains		
Mouse: K14CreER: Tg(KRT14-cre/ERT) 20Efu/J	Jackson Laboratory	Stock No: 005107
Mouse: Nat10$^{flox/flox}$	This study	N/A
Mouse: Nat10 conditional knockin	This study	N/A
Oligonucleotides		
qPCR primers of hGAPDH-R: ACCACCCTGTTGCTGTAGCCAA	This paper	N/A
qPCR primers of hGAPDH-F: GTCTCCTCTGACTTCAACAGCG	This paper	N/A
qPCR primers of hEGFR-F: AGGCACGAGTAACAAGCTCAC	This paper	N/A

REAGENT or RESOURCE	SOURCE	IDENTIFIER
qPCR primers of hEGFR-R: ATGAGGACATAACCAGCCACC	This paper	N/A
siNAT10: AATTCAGGATTTAGAGACTGG	This paper	N/A
tRNA-Gly-CCC: GTCTCCCACGTGGGAGGCGA	This paper	N/A
tRNA-Lys-CTT: AACGTGGGGCTCGAACCCAC	This paper	N/A
U6 snRNA: TGGAACGCTTCACGAATTTG	This paper	N/A
NAT10 sgRNA1-F: CACCgATCCGGATTCTCATTGAGAA	This paper	N/A
NAT10 sgRNA1-R: AAACTTCTCAATGAGAATCCGGATC	This paper	N/A
NAT10 sgRNA2-F: CACCGATCTCTCTTTGTTGTAGTT	This paper	N/A
NAT10 sgRNA2-R: AAACAACTACAACAAAGAGAGATC	This paper	N/A

RESOURCE AVAILABILITY

Lead contact
Requests for further information, data, and other resources can be directed to the lead contact, Shuibin Lin (linshb6@mail.sysu.edu.cn).

Materials availability
This study did not generate new materials.

Data and code availability
- All raw data of polyribosome-seq and ac4C-RIP-seq datasets generated during this study have been deposited on Gene Expression Omnibus (GEO): GSE225131 and are publicly available as of the date of publication.
- This paper does not report custom code.
- Any additional information required to reanalyze the data reported in this paper is available from the lead contact upon request.

EXPERIMENTAL MODEL AND SUBJECT PARTICIPANT DETAILS

Patient samples
All clinical samples mentioned in this study, including tissue chips and tissues for extracting RNA and protein, are derived from Sun Yat-sen University Cancer Center (Guangzhou, China). Informed consents were obtained from all patients. All patient-related studies were reviewed and approved by the Institutional Review Board of the hospital (Approval No: B2021-131-01). Clinical expression data of NAT10 transcription were obtained from The Cancer Genome Atlas (TCGA).

Xenograft mouse model
BALB/c nude mice were purchased from the Experimental Animal Center at the First Affiliated Hospital of Sun Yat-sen University (Guangzhou, China). Animal protocols were reviewed and approved by the Animal Care and Use Committee at the First Affiliated Hospital of Sun Yat-sen University (Approval No: 2021-855). The study conforms to the Animal Research: Reporting of In Vivo Experiments (ARRIVE). The committee limits tumor growth to no more than 10% of the animal's original body weight and the mean tumor diameter to no more than 20 mm. Mice were maintained under controlled conditions (12/12 h light/dark cycle [lights on at 8 am]; 23 ± 2°C; 55 ± 10% humidity; food and water ad libitum). For the subcutaneous implantation model, 5×10^6 TE9 or OE19 cells were injected into randomly grouped 6-week-old female BALB/c nude mice. The length (a) and width (b) of the tumors were measured at the indicated time points using calipers, and the tumor volumes (V) were calculated by the formula $V=1/2 \times a \times b^2$.

Generation of *Nat10* conditional knockout and conditional knockin mice

To generate *Nat10* conditional knockout mice, we conditionally knocked out exon 4 of *Nat10* using the CRISPR-Cas9 system. Deletion of exon 4 will result in a truncated protein of 71 aa (66 native aa plus 5 frameshift aa) and lead to nonsense-mediated decay. The size of intron 3 and intron 4 is large and both loxP sites are inserted into non-conserved regions that do not interfere with mRNA splicing. Cre-dependent *Nat10* knockout mice were then generated by using a CRISPR-Cas9 strategy. cKI mice were generated by ligating a synthetic *Nat10*-CDS fragment (3103bp, digested with AscI and EcoRV) to mROSA-KI-12p (digested with AscI and EcoRV), forming *Nat10* mROSA-KI-12p-A targeting vector, which was introduced into the ROSA 26 locus. The epithelial tissue-specific conditional knockout or knockin was achieved by crossing with Keratin14-CreER mouse and tamoxifen treatment.

METHOD DETAILS

Immunohistochemistry (IHC) staining

The immunohistochemistry was performed according to the kit instructions (Gene tech, China). Primary antibodies are as follows (Anti-NAT10, Proteintech, 1: 200 dilution; Anti-Ki67, Proteintech, 1:1000 dilution; Anti-EGFR, Proteintech, 1:2000 dilution). IHC staining was estimated using QuPath (v0.2.3) and presented as H-score. Tissues with H-score $\geq$ 120 were defined as high expression samples, while tissues with H-score below 120 were defined as low expression samples.

Cell culture

ECA109, TE13, and KYSE30 ESCA cells were purchased from Shanghai EK-Bioscience Biotechnology Co., Ltd. TE9 cells were from Lizu Wu lab. OE19 and OE33 cells were purchased from Shanghai Biowing Applied Biotechnology Co., Ltd. 293T cells were purchased from American Type Culture Collection (ATCC). All cells were cultured in DMEM (Gibco, USA) medium containing 10% fetal bovine serum (FBS, Gibco, USA), 1% Penicillin (Gibco, USA), and 1% streptomycin (Gibco, USA) in a water-saturated atmosphere under 5% CO_2 at 37°C in an incubator (Thermo Scientific, USA).

Knockout and overexpression of NAT10 in ESCA cells

Lentiviral vectors expressing lenticrispr_v2 against GFP (sgGFP) and NAT10 were purchased from Horizon Discovery, Inc. For lentivirus production, lenticrispr_v2 vector, packaging vector pCMV-ΔR8.9 and envelope vector pCMV-VSVG were co-transfected into 293T cells using Lipofectamine 2000 reagent (Invitrogen, USA). 48 hours after transfection, the packed viruses were collected and used to infect ESCA cells with 10μg/ml Polybrene (Solarbio, China), then 2.5μg/ml puromycin (Solarbio, China) was used to select infected cells 48 hours after infection. Small interfering RNA (siRNA) targeting NAT10 was used to knockdown NAT10 in puromycin intake assays. The NAT10 overexpression plasmid pICE-FLAG-NAT10-siR-WT (oeWT), and the functional mutation overexpression plasmid pICE-FLAG-NAT10-siR-G641E (oeMUT) were purchased from Addgene (https://www.addgene.org/). The plasmids were transfected into cells using Lipofectamine 2000 reagent according to the manufacturer's instructions.

RNA extraction and qRT-PCR

Trizol reagent (Invitrogen, USA) was used to isolate total RNA following the manufacturer's instructions. 2μg RNA was used for reverse transcription by HiScript III RT SuperMix for qPCR Kit (Vazyme, China). Next, the cDNAs were 1:20 diluted for qRT-PCR using TB Green™ Premix Ex Taq™ II (Takara, Japan) in StepOnePlus™ real-time PCR system (Thermo Scientific, USA). *GAPDH* was used as an internal control.

Western blot, northwestern blot, and northern blot

Western blot, northwestern blot, and northern blot assays were performed as previously reported (*8*). Briefly, for northern blotting, 10% TBE-UREA gel was used to separate 2μg RNA by electrophoresis. Then the separated RNAs were transferred onto a positively charged nylon membrane followed by cross-linking with Ultraviolet (UV) light. The tRNAs and U6 snRNA were blotted with corresponding digoxigenin-labeled probes. For northwestern blotting, after transfer and cross-linking, the RNA-containing nylon membranes were blotted with anti-ac4C antibody (Abcam, USA, 1:500 dilution). For anti-ac4C immunoprecipitation and tRNA northern blots, the tRNA were incubated with anti-ac4C antibody, then the immunoprecipitated RNA were subjected to northern blot assay with indicated probes.

Colony-formation, cell proliferation assays

For the cell proliferation assay, 1,000 ESCA cells were seeded into 96-well plate. Following the manufacturer's instructions, cell proliferation was analyzed within 5 days after implantation using Cell Counting Kit-8 (Dojindo, Japan). For colony-formation assay, 500 cells were seeded into 6-well plate and cultured for 12 days. The the cells were fixed with 4% paraformaldehyde for 30 min at room temperature and stained with 0.5% crystal violet solution. Finally, the results were statistically analyzed using ImageJ (version 1.53n).

Cell apoptosis assays

Cell apoptosis assay was performed using Annexin V-FITC Apoptosis Detection Kit (KeyGEN BioTECH, China) following the manufacturer's instructions. The percentage of positive cells was detected using CytoFLEX (Beckman Coulter, USA).

Puromycin intake assay

Cells were incubated with medium containing 1μM puromycin at 37°C for 30 min, followed by protein isolation and western blotting. The same samples were used for Coomassie Blue staining as reference for protein loading. Anti-puromycin antibody (MABE343, Millipore, 1:50,000 dilution) was used to detect the rate of new protein synthesis.

ac4C RNA immunoprecipitation sequencing (ac4C-RIP-seq)

Total RNAs were isolated using Trizol reagent (Invitrogen, USA) following the manufacturer's instructions. Small RNAs (17-200nt) were then purified using The RNA Clean and Concentrator-25 kit (ZYMO Research, USA). 20 μg small RNAs were incubated with 5 μl anti-ac4C antibody (abcam, USA) or IgG for 2 hours. The immunoprecipitated RNAs were isolated using Trizol reagent (Invitrogen, USA). The input small RNAs and immunoprecipitated small RNAs were treated with AlkB and AlkB-D135S and then used for cDNA library construction with Multiplex Small RNA Library Prep Set for Illumina Kit (New England Biolabs, USA) and subjected to high-throughput sequencing.

Analysis of ac4C-RIP-seq

For the ac4C-RIP-seq analysis, the human tRNA sequences containing the tRNA genes and 100 bp at both upstream and downstream were downloaded from GtRNAdb database (http://gtrnadb.ucsc.edu/genomes/eukaryota/Hsapi38/) as precursor tRNA genes. Then the introns were removed and a ''CCA'' sequence was added to the 3' end of each tRNA gene to constructing reference tRNA sequences. The raw sequencing data of our ac4C-RIP-seq were subjected to adaptor trimming and quality filtering (Q30), then the trimmed data were aligned to the reference tRNA sequences using Bowtie2 (http://bowtie-bio.sourceforge.net). The read count for each tRNA was calculated using the ARM-seq pipeline. tRNAs with counts > 15,000 in the input group of sgGFP were included for analysis. The rip ratio was calculated by the ratio of counts between ac4C and IgG group. The tRNAs with rip ratio > 2 in the sgGFP cells were defined as ac4C-modified tRNAs. The input group of sgGFP and sgNAT10 were used to study the effects of NAT10 in the expression levels of modified tRNAs.

Polyribosome-bound mRNAs sequencing (polyribosome-seq)

In short, cells were incubated with 100 μg/ml cycloheximide for 3 min and then treated with cell lysis buffer [1% Triton X-100 in ribosomal buffer (RB buffer) [200mM KCl, 15mM MgCl$_2$, 20mM HEPES-KOH (pH 7.4), 100μg/ml cycloheximide and 2mM dithiothreitol] on ice for 30 min. After centrifugation at 16,200 × g for 10 min at 4°C, the supernatant was transferred to the surface of 11 ml of sucrose buffer (30% sucrose in RB buffer). The polyribosome-bound mRNA was pelleted by ultracentrifugation at 185,000 × g for 5h at 4°C and purified using TRIzol reagent (Invitrogen, USA). cDNA library construction and sequencing were performed using the BGISEQ-500 platform (BGI, Shenzhen, China). Translation efficiency of a gene is calculated as the ratio of its transcript per million (TPM) in the polyribosome-seq to its TPM in the input RNA-seq. We first calculated the TPMs in the polyribosome-seq and the input RNA-seq separately, then compared the translation efficiency (Ratio) between different samples to analyze the changes of translation efficiencies of mRNAs in different samples.

Gene pathway enrichment analysis

Gene Ontology and Pathway Analysis were used for the pathway enrichment analysis. Differentially translated mRNAs identified in polyribosomal seq data and ribosome profiles were used for gene pathway analysis using the ToppFun module of the ToppGene Suite (https://toppgene.cchmc.org/enrichment.jsp). We classify genes with TE ≥ 2.5 as TE up and TE ≤ 0.4 as TE down. The rest are classified as TE non.

Hematoxylin and eosin stain (H&E) staining

In short, paraffin-embedded tissues were cut into 5-μm-thick sections. The sections were then baked at 65°C for 1 hour and dewaxed. The slides were washed with double distilled water and stained with hematoxylin and eosin. The sections were then dehydrated. Tumors in the ESCA mouse model were assessed according to H&E staining and graded as follows: showing signs of normal appearance (normal); epithelial dysplasia confined to the esophageal epidermis with indistinct basement membrane (dysplasia); loss of basement membrane with extensive invasion of the muscle layer (ESCA).

Inhibitor treatment *in vivo* and *in vitro*

In the *in vitro* experiments, remodelin (Sigma, USA) and gefitinib (Selleck, USA) were dissolved in DMSO, the concentration of gefitinib in the *in vitro* experiments was 20 μM and that of remodelin was 25 μM. Remodelin was administered by intraperitoneal injection at a dose of 4mg/kg body weight/3days. Gefitinib was administered at a dose of 80mg/kg body weight/3days by intraperitoneal injection. The drug injections lasted for two weeks in total.

QUANTIFICATION AND STATISTICAL ANALYSIS

All p-value calculations in this paper were performed by graphpad and SPSS. For histograms involved in the text, two tailed unpaired Student's t-test was used for p-value calculation and log rank test was used for survival curves. Figure 1F was determined with Pearson chi square test. The specific numerical values of the points in all figures are presented in source data.